

pubs.acs.org/Macromolecules Article

# Unexpected Gelation Behavior of Cellulose Nanofibers Dispersed in Glycols

Ruifu Wang, Hongrui He, Priyanka R. Sharma, Jiajun Tian, L. Daniel Söderberg, Tomas Rosén,\* and Benjamin S. Hsiao\*



**Cite This:** *Macromolecules* 2022, 55, 9527–9536



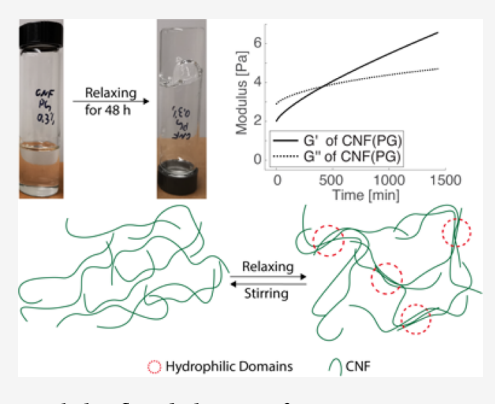
**ACCESS** I

III Metrics & More

Article Recommendations

s) Supporting Information

ABSTRACT: In this study, the gelation behavior of TEMPO-oxidized wood-based cellulose nanofiber (CNF) suspensions in two different glycols, ethylene glycol (EG) and propylene glycol (PG), was investigated near the overlap concentration and compared with that of aqueous CNF suspensions. The flow property of these non-aqueous and aqueous CNF suspensions was characterized by rheological, UV—vis, and rheo-optical techniques. It was found that the CNF(PG) suspensions exhibited stirring-reversible gelation behavior, where gelation could be induced simply by resting (i.e., prolonged holding time). However, this behavior was not observed for CNF(EG) and CNF(aq) suspensions. Higher temperature and higher CNF concentration could accelerate the gelation process of CNFs in PG, but no large-scale phase separation was detected by the optical techniques. Our study suggests that the reduced hydrophilic attraction between CNFs in PG is the main driving force for forming CNF-rich micro-domains, yielding a physically crosslinked



network. This study suggests that the choice of solvent can be used to tailor and control the flow behavior of CNF suspensions, leading to designs of new cellulose-enabled nanocomposites for varying applications.

#### ■ INTRODUCTION

As the world is facing unprecedented challenges of climate change and resource scarcity, the demand for renewable and environmentally friendly materials that can enable new circular economy increases. To tackle these challenges, cellulose, one of the most abundant natural-based polymers on earth, is an ideal candidate to serve as a scaffolding component to develop new materials that can replace existing synthetic plastics. Cellulose is the major component of all plant biomasses, including both woody and non-woody plants (e.g., trees, grasses, and shrubs), algae, and even certain animals and bacteria. Cellulose nanofibers (CNFs), the nanoscale aggregates of elementary building blocks from any higher plantcellulose microfibrils -can be extracted by combined chemical (e.g., TEMPO-mediated oxidation<sup>2,3</sup> and nitrooxidation<sup>4</sup>) and low-energy mechanical fibrillation (e.g., homogenization) methods. Materials from CNFs possess several unique properties, including high aspect ratio, high surface functionality (e.g., hydroxyl, aldehyde, and carboxyl groups), high Young's modulus, high hydrophilicity, and good aqueous dispersibility.<sup>1,5</sup> These properties make CNFs highly appealing in many applications, such as hydrogels, polymer reinforcements, 7,8 water-purification absorbents, and so forth.

Due to the high aspect ratio, dispersed CNFs can form a continuous fibrillar network in water above the critical concentration 10,11 due to the interaction and/or entanglement of adjacent nanofibers. The rheological behavior of macro- to

nano-scale fiber dispersions can generally be understood through a crowding factor, <sup>12,13</sup> describing the number of nearby fibers within a fiber's rotational volume. As CNFs in suspension generally possess surface charges (e.g., negative-charged carboxylate groups), the presence of cationic ions can further induce crosslinking effects. For example, the addition of monovalent cationic ions can screen the surface charge on cellulose and result in the aggregation of CNFs due to the increased hydrophobicity. The presence of multivalent cationic ions can result in ionic crosslinking between CNFs and yield an even stronger gel structure. <sup>14</sup>

Several interesting gelation phenomena have been observed in aqueous solutions of cellulose-based polymers. One system is methylcellulose (MC), where the hydroxyl groups (-OH) on the cellulose molecules are replaced by methoxide groups ( $-OCH_3$ ). MC exhibits a unique thermally reversible gelation behavior, that is, it forms a gel at high temperatures and returns to a shear-thinning suspension at low temperatures. <sup>15,16</sup> This property enables MC to be used in varying pharmaceutical, <sup>17</sup> cosmetic, <sup>18</sup> and cement applications. <sup>19,20</sup> The thermoreversi

Recived: May 18, 2022 Revised: August 19, 2022 Published: October 17, 2022





bility of MC in water can be attributed to its lower critical solution temperature (LCST) phase behavior. That is, at temperatures below the LCST, MC is soluble in water (or it becomes more hydrophilic); above the LCST, MC is insoluble in water (it becomes more hydrophobic). In other words, at high temperatures, the enhanced hydrophobicity of MC due to the methoxide groups triggers microphase separation and induces gelation, where the system exhibits significant increases in elasticity and storage modulus.

Unmodified cellulose can also show a gelation behavior in certain solvents. It has been reported that when cellulose is dissolved in a NaOH solution, the solution could form a gel at a prolonged holding time.<sup>22</sup> Furthermore, the gelation rate of this system was directly related to the temperature. Weng et al. attributed this gelation behavior to the perturbations of small molecules covering the cellulose chains at elevated temperatures.<sup>23</sup> They argued that when small molecules are perturbed, the hydroxyl groups on the cellulose molecules can aggregate and form random inter-chain junctions. However, unlike MC gel but similar to ion-induced CNF gels, these cellulose gels are thermally irreversible. In a related study, Roy et al. investigated the gelation behavior of 5 wt % cellulose in 9 wt % of NaOH solution.<sup>24</sup> They found that the storage modulus could gradually become higher than the timedependent loss modulus at a fixed oscillation frequency, indicating an irreversible gel formation. This gelation behavior was attributed to an unexpected phase separation event dictated by the interplay between hydrophilic and hydrophobic interactions.

Inspired by the above studies (thermally reversible gelation behavior in MC/water and thermally irreversible gelation behavior in cellulose/NaOH solution), we have investigated the gelation behavior of CNFs dispersed in different polar protic solvents: water, ethylene glycol (EG), and propylene glycol (PG) at varying temperatures. These solvents all possess an ability to form hydrogen bonds with CNFs but differ in terms of hydrophobicity, which is temperature-dependent. In the study, suspensions of wood-based TEMPO-oxidized CNFs in EG and PG were prepared through a solvent exchange process. The solubility of cellulose in these solvents has been characterized using the Hansen solubility parameter (HSP). Briefly, the general term of solubility parameter  $\delta_t$  (MPa $^{0.5}$ ) is defined as

$$\delta_t = \sqrt{\frac{E}{V}} \tag{1}$$

where E is the cohesion energy and V (cm³/mol) is the molar volume. Hansen separated the term E into three parts, dispersion interactions  $E_{\rm d}$ , dipole interactions  $E_{\rm p}$ , and H-bond interactions  $E_{\rm h}$ . The quantitative solubility of cellulose molecules in various solvents can be estimated using a value called interaction radius ( $R_{\rm a}$ ) with the following expression.

$$R_{a} = \sqrt{4(\delta_{d1} - \delta_{d2})^{2} + (\delta_{p1} - \delta_{p2})^{2} + (\delta_{h1} - \delta_{h2})^{2}}$$
 (2)

 $R_{\rm a}$  has the same unit as  $\delta$  and represents the distance between the HSP of solute and solvent in the 3-D HSP diagram. Conventionally, a smaller  $R_{\rm a}$  value indicates higher solvency power.

In this work, the rheological behavior of CNF(EG) and CNF(PG) suspensions was carefully characterized at different temperatures and different concentrations (i.e., from  $\sim$ 2 to  $\sim$ 3 mg/mL, or 0.2 to 0.3 wt %), where that of CNF dispersed in

water was also carried out as a reference. Complementary rheooptical measurements were performed to monitor the in situ
structural changes in CNF(EG) and CNF(PG) suspensions
through the flow-induced birefringence. Previously, we
observed that CNF suspensions in water and glycols (EG
and PG) behaved similarly to typical polymer solutions with a
solvent-independent overlap concentration. However, we
observed an unexpected stirring-reversible gelation behavior in
the CNF(PG) suspensions that could be induced simply by
resting, but this was not seen in the CNF(EG) suspensions.
This behavior was carefully investigated and explained by the
interplay between the hydrophobic/hydrophilic interactions
and the CNF surface charge capability in varying solvents,
concentrations, and temperatures.

#### EXPERIMENTAL SECTION

**Materials.** A commercially available TEMPO-oxidized cellulose nanofiber (CNF) aqueous slurry (concentration of 1.1 wt %) from the University of Maine was used as the base material. The CNF in this suspension had a carboxylate content of 1.5 mmol/g, and its morphological parameters were carefully characterized by Rosén et al. earlier. Regarding the chosen glycols: 1,2-ethanediol (EG) was obtained from Fisher Scientific and 1,2-propanediol (PG) was obtained from VWR. All chemicals and CNF suspensions were used without further purification. In addition, deionized water was used throughout the study.

Preparation of Cellulose Nanofibers in Different Solvents. An aqueous CNF suspension with a 3.4 mg/mL concentration was prepared by diluting the original CNF slurry. After the dilution, the suspension was passed through a homogenizer (PandaPlus, GEA Nitro Soavi) five times at a pressure below 200 bar to obtain the homogeneous CNF(aq) stock suspension. The suspension was then filtered through a 22  $\mu$ m filter paper to remove any large flocs. The final concentration of the CNF(aq) suspension was confirmed by the gravimetric analysis (Supporting Information).

The CNF suspensions dispersed in EG and PG, labeled as CNF(EG) and CNF(PG), were prepared according to our previous method. 11 Briefly, the CNF(aq) suspension was mixed with EG or PG in a 1:1 volumetric ratio to ensure the same final concentration of CNF(EG) or CNF(PG) was prepared as CNF(aq) (the densities of the suspensions were assumed to be the same as the corresponding solvents). In the solvent exchange process, water in the mixture was gradually removed by heating at 50 °C under reduced pressure, where the loss of EG or PG was assumed to be negligible. The CNF(EG)/ CNF(PG) suspensions at other concentrations were obtained by direct dilution of the CNF(EG)/CNF(PG) stock suspension. In this work, three concentrations of CNF(EG)/CNF(PG) suspensions were prepared: 3.4, 2.8, and 2.2 mg/mL, where the concentrations were also confirmed by the gravimetric analysis. Based on our earlier study, 11 the solvent exchange method effectively removed more than 98% of water, where the effect of residual water (less than 2%) on the rheological behaviors of CNF suspensions in EG and PG was very

**Ultraviolet–Visible Spectroscopy.** Ultraviolet–visible (UV–Vis) spectroscopy of 3.4 mg/mL CNF(PG) suspension was carried out using a ThermoFisher GEN10S spectrometer at room temperature. The scanning wavelength was from 400 to 760 nm, covering the visible light range, with an interval of 1 nm. The CNF(PG) suspensions were measured directly after stirring at 400 rpm for 30 min and subsequent aging at 0.5, 1, 3, 7, 24, and 30 h, respectively. Pure PG was used to obtain the background of the spectra.

**Zeta-Potential Measurement.** Zeta-potential measurements of CNF(aq), CNF(EG), and CNF(PG) suspensions at 3.4 mg/mL were conducted by a NanoBrook Omni Analyzer (Brookhaven instrument Inc.). The final results of each sample were averaged over at least five repetitions. Pure water, EG, and PG were also characterized to provide the background data.

**Rheological Measurements.** Rheological measurements were performed using an Anton Paar Physica MCR-301 stress-controlled rheometer with a concentric geometry using an operational gap of 1.12 mm. Several different types of measurement protocols were used to investigate the rheological properties of CNF(EG) and CNF(PG) suspensions in detail, which are described below.

**Long-Time Oscillation Monitoring.** The oscillation mode was used to identify the onset of the gelation process of CNF(PG) at different concentrations. In comparison, CNF(EG) was studied under the same protocol [CNF(aq) was skipped due to the weak response signals and the relatively low machine sensitivity]. The frequency was set to 1 Hz and the strain at 1%. The total experiment was carried out for 24 h. The samples were stirred at 400 rpm for 20 min and equilibrated at 25 °C for 3 min before the measurement.

**Relative Shear Viscosity Evaluation.** A measurement was performed to determine the relative viscosity ( $\eta_{\rm rel} = \eta_{\rm solution}/\eta_{\rm solvent}$ ) of the different CNF suspensions. In this measurement, CNFs dispersed in water, EG, and PG were diluted to ~0.3 mg/mL (below the overlap concentration) and then sheared at a fixed shear rate of 0.1 s<sup>-1</sup> for 16 min. The viscosity corresponding to this shear rate can be considered as the zero-shear viscosity.

**Temperature Scanning.** The effect of temperature was studied in two ways. In the first approach, the experimental procedure was similar to the long-time oscillation monitoring experiment. In brief, the long-time oscillation measurement was conducted for CNF(PG) suspensions at different concentrations but under varying temperatures, ranging from 15 to 60 °C. This measurement allowed us to develop the relationship between gelation time and temperature. In the second approach, a temperature sweep at a rate of 1.5 °C/min from 25 to 67 °C was performed for CNF(PG) and CNF(EG) suspensions at 3.4 mg/mL. During the sweep, the oscillation measurement was performed at 1 Hz and 1% strain. All the samples were stirred at 400 rpm for at least 20 min and equilibrated at 25 °C for 3 min before the measurement.

Rheo-Optical Characterization. A custom-built flow cell designed by Rosén et al.<sup>28</sup> was used to study the homogeneity of CNF(PG) and CNF(EG) suspensions before and after the gelation process using an in situ flow-induced birefringence technique. In this cell, a straight 1 mm wide square channel sandwiched between two layers of transparent cyclic olefin copolymer (COC) films (Tekni-Plex 8007 X-04, 150  $\mu$ m thickness) was used to detect the optical signals in operando, that is, under flowing conditions. The cell was placed between two linear polarizing films, with the polarization angles being +45 and -45° against the flow direction (Figure S1, Supporting Information). The light source was provided by a 635 nm red laser [635ML(60)-3-1235, Laserland] having an illumination size of around 1.4 cm. The transmitted optical images were recorded by a monochrome camera (Mako U-029b, Allied Vision). Optical images from the stable flow of the CNF(EG) and CNF(PG) suspensions (3.4 mg/mL, after 400 rpm of stirring) at a rate of 3 mL/h were first recorded as the references (at a rate of 100 frames per second). The flow profile was allowed to develop for 1 min prior to video recording. Afterward, the CNF suspensions were stopped and rested inside the flow cell for 24 h before the flow was restarted at the same flow rate for measurements. The image acquisition at 50 frames per second was adopted after the 24 hour rest. The recording was started 5 s before the flow was restarted. The exposure time during the measurement was fixed at 0.2 ms for all experiments.

#### ■ RESULTS AND DISCUSSION

Unexpected Gelation Behavior in CNF(PG). Immediately after the 30 min of mechanical stirring at 400 rpm, both CNF(PG) and CNF(EG) suspensions (3.4 mg/mL, measured by the gravimetric analysis) showed good homogeneity on the macroscopic scale, where no agglomerations or precipitations could be visually observed. These samples exhibited good flowability similar to the CNF(aq) suspension at the same concentration. Interestingly, after standing (resting) at room

temperature for more than 48 h, CNF(PG) suspensions exhibited a strong gelation behavior and resistance to gravity-driven flow. However, this unexpected gelation was not seen in CNF(EG) and CNF(aq). These results are illustrated in Figure 1, where photographs of CNF suspensions in varying solvents

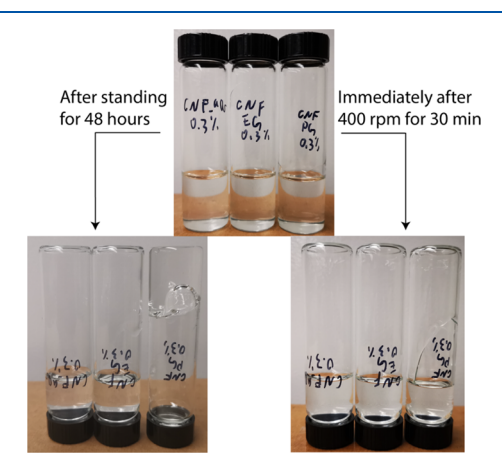


**Figure 1.** Reversing test of CNF dispersed in water (left), EG (middle), and PG (right) at 3.4 mg/mL directly after stirring (upper right figure) and after standing (resting) for 48 h (lower right figure).

subjected to a reversing test are shown. However, we noticed that the arrested CNF(PG) could easily return to the suspension state by mechanical stirring, indicating that the gelation of CNF(PG) is fully reversible and induced by physical interactions, which inspired the study.

To investigate the unexpected gelation in CNF(PG) simply by resting, rheological measurements were carefully carried out using different protocols. First, the long-time oscillatory deformation on CNF(PG) and CNF(EG) was carried out, where results are shown in Figure 2. In this figure, the storage

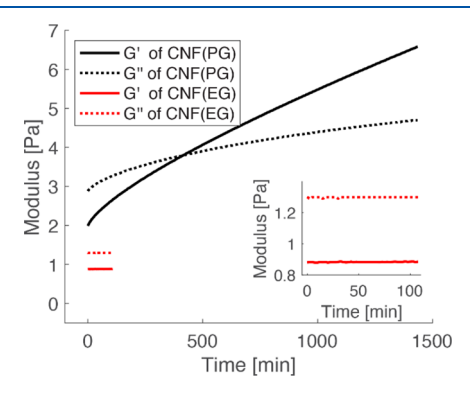


Figure 2. Storage modulus (G') and loss modulus (G'') of CNF(PG) and CNF(EG) at a concentration of 3.4 mg/mL at 25 °C. The inset figure shows the zoomed-in data of G' & G'' for CNF(EG).

modulus (G') and loss modulus (G'') of CNF(PG) and CNF(EG) at 3.4 mg/mL at 25 °C and 1 Hz of oscillation frequency were shown as a function of time [CNF(aq) was skipped due to machine sensitivity]. It was seen that in CNF(PG), both G' and G'' were increasing with time but at different rates. In the beginning, the sample behaved similar to a conventional polymer solution, with G' smaller than G''. However, with the increase in holding time, G' increased twice more rapidly than G'' (the cross-over time was around 420

min). The ratio between the slopes of G' and G'' was approximately 3 after 24 h of holding.

The gelation point, as defined by Winter and Chambon, <sup>29</sup> is where the ratio of G' and G'', after scaled with  $\omega^n$  (n is in the range of 0 < n < 1), becomes frequency-independent. <sup>23</sup> Due to the high solvent viscosity of PG, the dispersed CNFs in PG would experience much slower Brownian dynamics than those in EG or water and require days to achieve an equilibrium state. In this case, the cross-over time (the time where G' = G'') measured at the constant oscillation frequency was chosen as the nominal gelation time, <sup>22–24,30</sup> and the loss tangent  $\tan \delta = G'/G''$  was used to determine if the state is either a suspension ( $\tan \delta > 1$ ) or a gel ( $\tan \delta < 1$ ). We note that this criterion is frequency-dependent, <sup>30</sup> so a frequency of 1 Hz was fixed for all the samples tested here. Based on this criterion, the CNF(PG) suspension at 3.4 mg/mL could form a loose gel after ~420 min of holding time.

In Figure 2, the CNF(EG) suspension does not show any noticeable modulus changes during the experiment (the inset of Figure 2 only displayed the initial results), with G' being constantly smaller than G''. This indicates that the CNF(EG) suspensions behaved similar to a typical polymer solution without the transition to gel state as CNF(PG). The observation suggests that the gelation transition of CNFs in suspension is closely related to the solvent property, which will be carefully discussed later. A cursory consideration could be that the strong dissociation of carboxylated groups on the surface of CNFs in an aqueous environment causes strong electrostatic repulsion, preventing fiber-fiber contacts and leading to reduced entanglement of CNFs.<sup>2</sup> As glycols (EG and PG) possess much lower dielectric constants, they would significantly suppress the dissociation of carboxylated groups on CNFs, providing the opportunity for CNFs to aggregate and entangle. Furthermore, one hypothesis is that CNFs in EG and PG are more flexible than in an aqueous environment because there are no contributions from electrostatic repulsion to the bending stiffness.<sup>31</sup>

Temperature Effect on the Gelation Behavior. The temperature dependence of the loss tangent tan  $\delta$  of CNF(PG) and CNF(EG) at 3.4 mg/mL was investigated by applying a 1.5 °C/min of reversible temperature sweep protocol, where the result is shown in Figure 3 [the actual data of G' and G'' of CNF(PG) can be found in Figure S2, Supporting Information]. With the increase in temperature, the loss tangent continued to decrease for CNF(PG) and passed through the gelation point at  $\sim 52$  °C (the loss tangent = 1), as shown in Figure 3a. However, when the temperature started to decrease, the loss tangent was still less than 1 but decreased slightly and reached a plateau value of ~0.6 [i.e., CNF(PG) remained in a gel state]. This experiment indicated that CNF(PG) gelation is thermally irreversible, that is, very different from the thermoreversibility observed in the MC solutions. 16,18 In contrast, the loss tangent of CNF(EG) was completely different from CNF(PG) during the temperature sweep experiment. In Figure 3b, CNF(EG) was viscous-fluid-like, with the increase in loss tangent at higher temperatures (loss tangent values are all larger than 1). Moreover, the temperature sweep measurement of CNF(EG) indicated that its responses are completely reversible. We note that the viscosity of PG is ~44 mPa·s, which is about ~3 times larger than EG and ~50 times larger than water. Thus, the phenomenon may not be only due to the slower Brownian dynamics of CNFs in PG

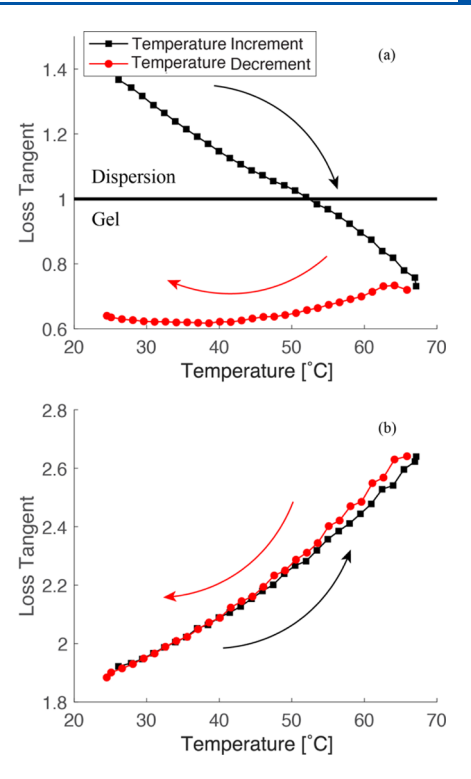
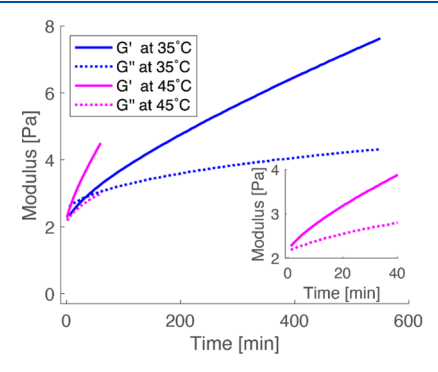


Figure 3. Loss tangent of (a) CNF(PG) and (b) CNF(EG) at 3.4 mg/mL as a function of temperature (the temperature sweep rate = 1.5 °C/min; frequency = 1 Hz).

than in EG. This effect of the solvent viscosity is considered next.

Figure 4 shows the G' and G'' values of CNF(PG) (3.4 mg/mL) at 35 and 45 °C (the data at 20 and 30 °C are shown in



**Figure 4.** G' and G'' values of CNF(PG) (3.4 mg/mL) at 35 and 45 °C. The inset figure shows the enlarged data frame at 45 °C [the cutoff of CNF(PG) at 45 °C is because no significant features could be observed at longer times].

Figure S3, Supporting Information) to investigate the effect of temperature on the rheological properties. All rheological results exhibited the behavior of gel formation (from a solution state at the initial stage to the arrested gel state at the later stage) except for CNF(PG) at 45 °C, which showed an immediate gel behavior (i.e., G' > G'') at the start of the experiment. However, considering the initial viscous fluid-like behavior of CNF(PG) after the sample preparation and the experimental setup time, we estimated that CNF(PG) started the gel formation at around 5 min at 45 °C. In Figure 4 and Figure S3 (Supporting Information), the G' value of CNF(PG) was found to increase continuously with time, similar to an

Table 1. Gelation Time  $t_{gel}$  (in min) of CNF(PG) at Different Concentrations and Temperatures (Frequency Was 1 Hz)<sup>a</sup>

	conc (mg/mL)	20 °C	25 °C	30 °C	35 °C	40 °C	45 °C	50 °C	55 °C	60 °C
	3.4	932	470	161	35	initial gel	initial gel			
	2.8		too long	1695	670	111	70			
	2.2					too long	681	465	114	46
c	Unit: min.									

early report by Roy et al.  $^{24}$  Unfortunately, the G' value did not reach a plateau during our chosen experiment condition. We believe that the primary factor is the low electrostatic dissociation of CNF in PG, which can induce the microphase separation and result in higher elasticity of the network structure in a gel, associated with the hydrophobicity of the solvent which also play a role to cause the viscoelasticity difference between CNF(EG) and CNF(PG), and this will be discussed later. The observed gelation times  $t_{\rm gel}$  for CNF(PG) at different concentrations and temperatures (frequency was 1 Hz) are shown in Table 1. It was interesting to note that the gelation time decreased with the increase in temperature. This is reasonable as the Brownian motions of CNF particles increase with temperature, which can trigger a faster process toward the equilibrium state, or gelation state, in other words. In contrast, the high electrostatic dissociation of CNF in EG will hinder the gelation process of CNFs due to the electrostatic repulsion. Furthermore, we expect the effect of temperature on the electrostatic dissociation of CNF in varying solvents, if any, to be very small.

Concentration Effect on the Gelation Behavior. The effect of the concentration on the gelation behavior of CNF(PG) was also investigated. The G' and G'' values as a function of time at 25 °C and 1 Hz for CNF(PG) suspensions at three different concentrations (i.e., 2.2, 2.8, and 3.4 mg/mL) are shown in Figure 5. At a concentration of 2.2 and 2.8 mg/

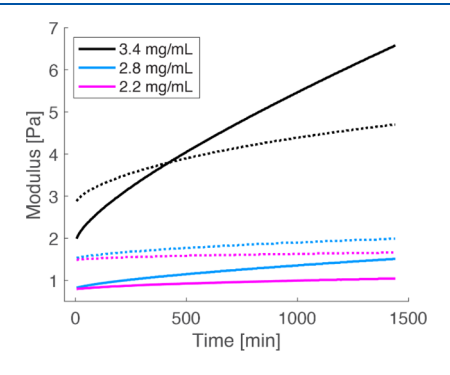
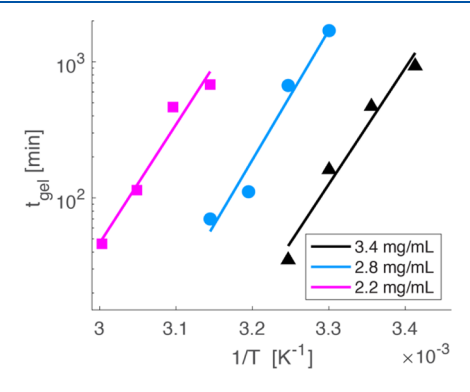


Figure 5. G' (solid line) and G'' (dash line) values of CNF(PG) in various concentrations and at 25 °C.

mL, respectively, the time-induced gelation behavior was weak but still evident even though the cross-over time could not be determined under the chosen time span (24 h). It was found that the G' and G'' values in less concentrated CNF(PG) were much smaller than those of CNF(PG) at 3.4 mg/mL, which could be attributed to the looser network structure of CNFs. The time-dependent G' and G'' cross-over transition, that is, gelation time, of CNF(PG) at 2.2 and 2.8 mg/mL could be observed at higher temperatures (Table 1). For example, the gelation time of CNF(PG) of 2.8 mg/mL at 30 °C was around 1695 min, and it became around 70 min at 45 °C; the gelation time of CNF(PG) of 2.2 mg/mL at 45 °C was around 681 min (Figure S4, Supporting Information), and it became around 46 min at 60 °C. The gelation time of CNF(PG) always decreased with the increase in temperature, indicating an enhanced Brownian motion of CNF, which promotes gelation formations of CNFs (i.e., forming physical network points). The steady increase of the G' value indicated that none of the CNF(PG) suspensions had reached their equilibrium state, likely due to the slow Brownian dynamics caused by the high viscosity of

The gelation time and temperature for CNF(PG) at different concentrations have an interesting relationship. Figure 6 shows the semi-log plot of the gelation time as a function of



**Figure 6.** Dependence of gelation time on temperature for CNF(PG) in various concentrations along with the exponential fitting (t stands for time and *T* stands for temperature).

temperature for varying CNF(PG) suspensions, which exhibits a linear relationship. All three CNF(PG) suspensions at different concentrations clearly showed an exponential dependency of the temperature (R2 larger than 0.93) with a similar slope (between -0.19 to -0.23, depending on concentration). These results are consistent with those observed by Roy et al., <sup>24</sup> who reported a slope around -0.4. This slope difference is likely due to the completely different cellulose systems investigated in their work. In addition, the cellulose solutions studied by Roy et al. were at much higher concentrations and had no chemical modification compared to nanocellulose. It is reasonable to assume that different aspect ratios and physical properties of cellulose fibers can lead to very different gelation behaviors.

The Arrhenius equation was used to describe the temperature dependence of gelation time (reversely proportional to gelation rate) of CNF(PG) suspensions at different concentrations

$$\ln(t_{\text{gel}}) = \frac{E_{\text{a}}}{RT} + \text{Const}$$
(3)

where  $E_a$  is the activation energy, R is the gas constant, and T is the temperature in Kelvin. The Arrhenius plot of  $ln(t_{gel})$ versus 1/T is shown in Figure S5 (Supporting Information), where the slopes are also indicated. The activation energies from three CNF(PG) suspensions at different concentrations

are summarized in Table 2. It was interesting to note that, considering the experimental error, the three estimated

Table 2. Activation Energy of CNF(PG) at Different Concentrations (Calculated Through Gelation Time Using the Arrhenius Equation)

conc. (mg/mL)	2.2	2.8	3.4
activation energy (kJ/mol)	$167 \pm 25$	$182 \pm 27$	$164 \pm 22$

activation energy values seem to be the same, with the mean value around 170 kJ/mol. This suggests that the required temperature to increase the Brownian motion of CNF to trigger the gelation process in the suspensions of different concentrations (all above the overlap concentration) is basically the same.

**UV–Vis and Rheo-Optical Investigation.** Many reports mentioned that the gelation behavior in cellulose solutions is caused by the microphase separation between the cellulose chains and the solvent molecules, where reduced light transmittance or turbidity can be detected by optical techniques. This indicates that the domain size of the microphase is in the range of the wavelength of visible light. However, in our system, this was not the case. Figure 7 shows

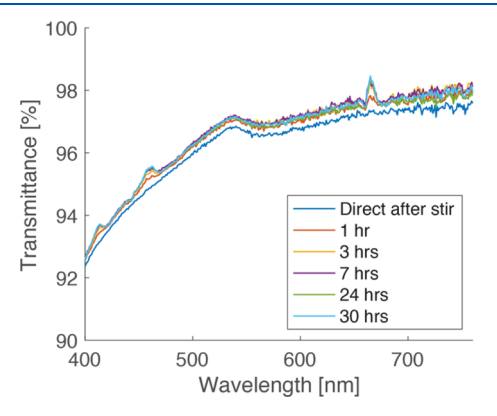


Figure 7. UV—visible spectroscopy of CNF(PG) at 3.4 mg/mL after various resting times.

the transmittance in the visible light range for CNF(PG) at 3.4 mg/mL at a varying resting time (up to 30 h) at room temperature. It was seen that the CNF(PG) suspension maintained very high transmittance (>90%) in the wavelength range of 400–760 nm without obvious change. Considering that the gelation time of CNF(PG) at 3.4 mg/mL is around 7 h at room temperature, the network structure in CNF(PG) is clearly below the wavelength of the visible light and leads to reduced transmittance. This can be explained by the fact that the relatively low Brownian motion of the PG molecules could hinder the CNF translation movement, where the gel domains of CNFs were confined locally. With higher temperatures, a higher degree of segmental aggregation can occur, forming a LCST-like phase separation behavior.

Because CNFs are birefringent, it is possible to study their hydrodynamic alignment through rheo-optics. This technique has been demonstrated as a powerful tool to study in situ structural/morphological changes in semi-crystalline polymer melts/solutions under varying flow fields, <sup>33,34</sup> where segmental chain aggregation can lead to crystallization. The flow-induced birefringence of CNF(EG) and CNF(PG) at 3.4 mg/

mL, along with the transmitted intensity under cross-polarized conditions versus time using a custom-built flow cell, are shown in Figure 8 (the complete videos are shown in Videos S1, S2, S3, and S4 in Supporting Video). In this measurement, two positions at the center and edge of the channel were selected, respectively, for the transmitted intensity measurement. During the steady-state flow condition, that is, the samples were pumped immediately after the severe stirring (upper images in Figure 8a,d), both CNF(EG) and CNF(PG) showed similar flow behaviors, where the bright regions close to the channel walls represent aligned CNFs due to the strong shear rates. The corresponding transmitted intensity at the two selected positions (center and edge) under cross-polarized conditions are shown in Figure 8b,e. It was interesting to note that the intensity profile of CNF(PG) exhibited certain fringes at the edge, making the intensity fluctuate (Figure 8c), which could be due to the inhomogeneity in the macroscale, whereas CNF(EG) showed good homogeneity with stable intensity (Figure 8b).

Interestingly, because of the natural birefringence of the COC films (the windows of the flow cell) being in the opposite direction compared to the aligned CNFs, the flow restart was accompanied by an intensity decrease, as shown in Figure 8c at  $\sim$ 25 s (the flow was started after 5 s, as marked in Figure 8c,f) and could be used to judge the actual starting of the flow. After resting inside the channel for 24 h, CNF(PG) took ~35 s to flow again, whereas CNF(EG) only took ~20 s. It was noticed that CNF(PG) restarted as a plug flow, with dark unaligned gels moving as an entity, indicating the existence of a wall-slip layer inside the channel (Video S4 at Supporting Video). While before the flow restarted, CNF(PG) exhibited higher intensity at the center position than at the edge. This is likely because CNFs were pre-aligned at the edge by the previous flow, with the unexpected gelation hindering a return to isotropy. As the dark unaligned region was continuous without observation of small isolated "islands", the formed CNF(PG) gel was a continuous phase. Gradually, the CNF close to the wall became brighter, which could be attributed to the total stress (represented by the total del deformation inside the channel) that went beyond the yield stress of the gels and caused local alignment. Because the shear effect was relatively weak (CNFs at the center positions were still under the plug flow, as seen in Figure 8d), a large amount of random CNF gel domains remained intact, which prevented CNF(PG) to restore back to the steady flow and resulted in the severe intensity fluctuation after ~100 s (Figure 8f). On the other hand, CNF(EG) did not exhibit any plug flow and could restore back to the steady flow after 90 s, quite different from the behavior of CNF(PG).

Discussions and Possible Gelation Mechanism. To explain the different gelation behaviors of CNFs dispersed in EG and PG, the solvent effect should be considered. According to the interactions between the solvent and polymer chains, solvents are divided into good and poor solvents. In a good solvent, polymer chains tend to interact favorably with the solvent molecules and become more extended, resulting in a larger excluded volume. In contrast, polymer chains in a poor solvent collapse. On the other hand, relative viscosity ( $\eta_{\rm reb}$  defined by the suspension viscosity divided by the solvent viscosity) could be used to identify the solvent effect. In polymer solutions, when the concentration is below the overlap concentration ( $C^*$ ) where the chain entanglement is not a dominant factor, a higher  $\eta_{\rm rel}$  value can be obtained in a

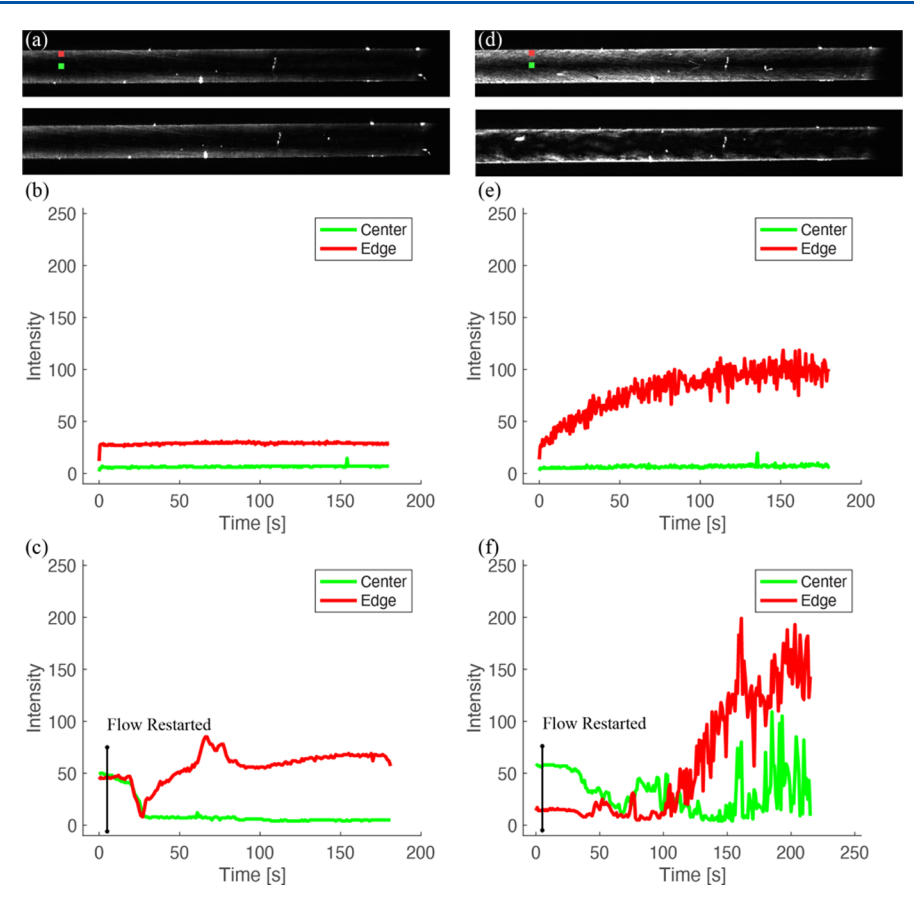


Figure 8. Flow behavior of CNF(EG) and CNF(PG) at 3.4 mg/mL. (a,d) Flow diagram at 150 s after the steady-state flow (upper) and samples rested in the channel for 24 h (lower). The red and green markers indicate the positions where the transmitted intensity under cross-polarized conditions was recorded; (b,e) plot of the intensity vs time for the steady-state flow of CNF(EG) and CNF(PG) at the center and edge positions, respectively; and (c,f) plot of the intensity vs time for CNF(EG) and CNF(PG) rested inside the channel for 24 h at the center and edge positions, respectively (the intensity was recorded 5 s before the flow initiation).

good solvent (or a lower  $\eta_{\rm rel}$  value is obtained in a poor solvent). This is because the extended polymer chains in a good solvent would have a higher chance to be in contact with each other and thus cause a higher solution viscosity, while the collapsed polymer chains in a poor solvent can result in a reduced probability of interactions.

Although CNFs can only form suspensions (not real solutions) in the chosen solvents, there are some similarities between nanofibers and polymer chains, where the general theoretical considerations for polymer solutions can still be adopted to CNF suspensions. The  $\eta_{\rm rel}$  values of CNF(aq), CNF(EG), and CNF(PG) in 0.34 mg/mL are shown in Table 3. It is evident that water is the best dispersing solvent for CNF, while PG is the poorest, which is expected because water introduces electrostatic repulsion, resulting in a larger excluded volume. More importantly, considering the structural difference between EG and PG, the extra methyl group on PG indicates that PG is more hydrophobic than EG. We suggest

Table 3. Relative Viscosity of CNF(aq), CNF(EG), and CNF(PG) at a Concentration of 0.34 mg/mL

	CNF(aq)	CNF(EG)	CNF(PG)
solvent viscosity (Pa*s)	$8.9*10^{-4}$	0.016	0.044
relative viscosity	1.79	1.56	1.40
dielectric constant	79	37	32

that this is the key to the observed unexpected gelation behavior of CNF(PG).

However, the consideration of HSP appears to provide the opposite picture. Table 4 shows the values of  $\delta_d$ ,  $\delta_v$ , and  $\delta_h$  for

Table 4. Solubility Parameters of Various Solvents and CNC, as Well as the Ra Values for CNC(aq), CNC(EG), and CNC(PG)

	$\delta_{\mathrm{d}}~(\mathrm{MPa}^{0.5})$	$\delta_{\rm p}~({ m MPa}^{0.5})$	$\delta_{\rm h}~({ m MPa}^{0.5})$	$R_{\rm a}~({\rm MPa}^{0.5})$
EG	17.0	11.0	26.0	14.4 (CNC(EG))
PG	16.8	9.4	23.3	13.8 (CNC(PG))
water	15.6	16.0	42.3	27.8 (CNC(aq))
$\frac{\text{CNC}(110)}{(1\overline{1}0)}$	18.1 ± 0.5	$20.4 \pm 0.5$	$15.3 \pm 0.4$	

EG, PG, water,<sup>37</sup> and cellulose nanocrystals (CNC),<sup>38</sup> another type of nanocellulose with surface charges, as well as the  $R_a$  values for CNC(aq), CNC(EG), and CNC(PG). Interestingly, CNC(PG) was calculated to be 13.8 MPa<sup>0.5</sup>, which is much smaller than 27.8 MPa<sup>0.5</sup> obtained from CNC(aq). Although the CNC and CNF are different in morphology, we expect CNFs would exhibit similar results. Based on the  $R_a$  results, Table 3 indicates that the dispersion of nanocelluloses in water is more difficult than dispersion in EG or PG. However, this

prediction ignored the behavior of electrostatic dissociations on the CNF surface in a different solvent. Specifically, the HSP approach does not consider electrostatic interactions, which have proven to be a dominating factor in the dissolution of polyelectrolytes in water.<sup>39</sup>

To deal with the issue of electrostatic dissociations on CNFs in varying solvents, the zeta-potential was measured to evaluate the charge dissociation of the suspensions. The zeta-potential values of CNFs dispersed in different solvents are shown in Table 5 (the concentration deviation was ignored). From this

Table 5. Zeta-Potential Values of CNFs in Different Solvents at Similar Concentrations

sample	zeta-potential (mV)	conc. (mg/mL)
CNF(aq)	$-83.9 \pm 2.1$	3.5
CNF(EG)	$-63.3 \pm 18.4$	3.5
CNF(PG)	$-18.2 \pm 10.8$	3.4

table, CNF(PG) was found to possess the lowest zeta-potential, indicating that the electrostatic dissociation on CNFs is only partially stabilized, similar to a report published by Isogai et al. <sup>39</sup> Due to the low zeta-potential value, the repulsion forces between CNFs are low. The low electrostatic dissociation of CNF in PG is one of the primary reasons for the unexpected gelation observed in CNF(PG) because the low repulsion forces between CNFs lead to strong interfibrillar interaction and formation of network entanglement. From the HSP consideration, we argue that PG will be a better solvent than water to disperse CNFs if one can exclude the electrostatic dissociation factor. One way to verify this hypothesis is to fabricate the CNF with different charge densities and extrapolate the  $\eta_{\rm rel}$  value at zero charge density, which is considered out of scope for the present work.

Based on the experimental results observed, we proposed a mechanism of unexpected gelation behavior of CNF(PG), where a schematic illustration of the proposed mechanisms is shown in Figure 9. In Figure 9, under the well-stirred condition, CNFs are well dispersed in PG (Figure 9 left), but the suspension is far away from the equilibrium state. Because of the difference in hydrophilicity between CNF and PG, CNFs tend to attract each other due to their similarity (e.g., polar carboxylated groups). However, the attractive interaction between CNFs is hindered by the high viscosity of the PG medium. As a result, fewer contact points (segmental aggregation) between CNFs are formed, resulting in a low G'

value. However, with the increase in holding or resting time, the Brownian motion of CNFs will eventually overcome the viscosity barrier of the dispersing solvent, slowly forming segmental aggregations (Figure 9 right) and creating a gel state representing the equilibrium state. The increase in the density of the micro-domains due to hydrophilic aggregation between CNF segments (as compared with the more hydrophobic PG) can increase the strength of this physical gel, as seen by the continuous increase in the G' value. However, these microdomains formed in the CNF(PG) gel are relatively small, revealed by the UV-vis spectrum, and contain mainly hydrophilic attractive interaction through van der Waals forces. These domains can be destroyed by sufficiently strong shear (rigors stirring), thus exhibiting a mechanical reversible gelation behavior. While in more hydrophilic, more polar EG, a stronger electrostatic dissociation and relatively strong hydrophilic interaction between CNF and EG prevent the formation of the segmental aggregation. CNF dispersed in water has a similar explanation.

The increase in temperature can enhance the Brownian motions of both CNFs and PG molecules, increasing the events of hydrophilic attraction between CNFs and lowering the viscosity barrier imposed by PG. This would accelerate the gelation process and reduce the gelation time in CNF(PG). In a way, the CNF(PG) suspension exhibits the LCST behavior, which is similar to the two cellulose solutions discussed earlier.  $^{16,22}$ 

Finally, in our experimental protocol, we have chosen only the frequency of 1 Hz and strain of 1% for all the samples to determine the crossing point (or the gelation point) between G' and G''. We note that such a crossing point depends not only on the time but also on the frequency, strain, and strain rate. For this reason, we have also carried out a frequency sweep experiment on the arrested 3.4 mg/mL CNF(PG) suspension at 25 °C under a similar strain (1.15%). It was seen that this suspension behaved similar to a conventional gel at all frequencies, that is, the G' is greater than G'' (Figure S7, Supporting Information). However, the gelation behavior was found to increase with the increase in frequency. This can be understood by the notion that once the gelation network is formed, the nanofibrous network can become more rigid at higher frequency of deformation which is expected.

#### CONCLUSIONS

The rheological behavior of TEMPO-oxidized cellulose nanofibers (CNFs) dispersed in EG and PG near the overlap

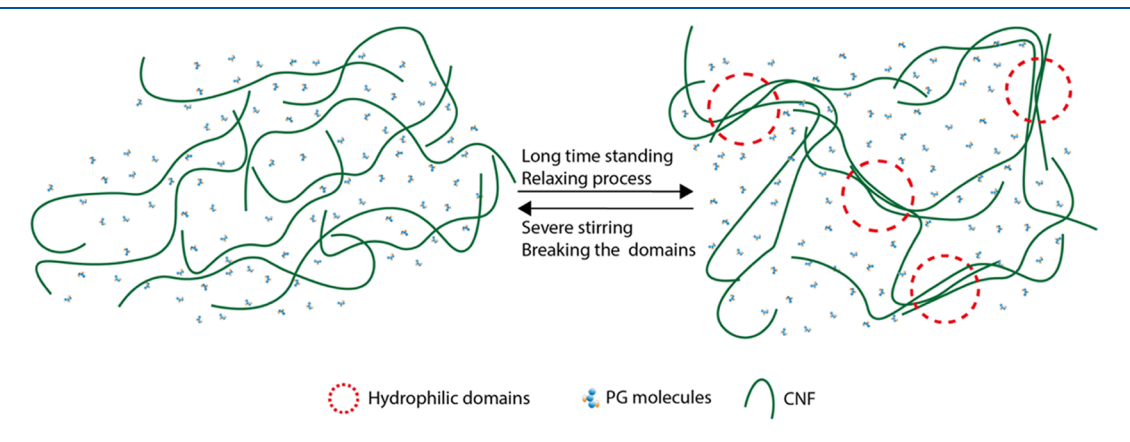


Figure 9. Schematic illustration of the proposed mechanisms underlying the unexpected gelation of CNF dispersed in PG.

concentration C\* under oscillatory shear was systematically studied. The CNF(PG) system showed an unexpected gelation behavior simply by resting, whereas CNF(EG) and CNF(aq) did not exhibit this behavior and acted as a conventional polymer solution. The unexpected gelation behavior in CNF(PG) is due to the combined effects of (1) low electrostatic dissociation of CNFs in PG, which reduces the interfibrillar repulsion and facilitates the formation of hydrophilic aggregation of CNFs, and (2) the relatively high concentration of the CNF suspension above C\*. However, the high viscosity of PG retards the segmental aggregation rate in CNFs. The gelation time of CNF(PG) was found to be a function of CNF(PG) concentration and temperature. The semi-empirical analysis of the relationship between the gelation time and temperature indicated a constant exponential factor of ~0.2. This relationship was further analyzed by the Arrhenius equation, yielding a constant activation energy of around 170 kJ/mol for all CNF(PG) at different concentrations (all above the overlap concentration). These results indicate that the CNF(PG) suspension (>C\*) possesses two unique features: (1) the mechanical reversible gelation behavior-gelation can be induced by resting and destroyed by mechanical perturbation and (2) the LCST-like behavior solution-like behavior at low temperatures and gel-like behavior (thru segmental aggregation of CNFs) at high temperatures.

#### ASSOCIATED CONTENT

#### Supporting Information

The Supporting Information is available free of charge at https://pubs.acs.org/doi/10.1021/acs.macromol.2c01035.

Description of gravimetric measurement, rheo-optical device, wide-angle X-ray diffraction (WAXD) and rheological frequency sweep experiment, temperature effect on G' and G'' of CNF(PG) at 1 Hz, WAXD measurements of dried samples from CNF(PG) and CNF(aq), and rheological frequency sweep results from CNF(PG) (PDF)

Flow of CNF(EG) after stirring (AVI)

Flow of CNF(EG) after overnight standing (AVI)

Flow of CNF(PG) after stirring (AVI)

Flow of CNF(PG) after overnight standing (AVI)

#### AUTHOR INFORMATION

#### **Corresponding Authors**

Tomas Rosén — Fiber and Polymer Technology Department and Wallenberg Wood Science Center, KTH Royal Institute of Technology, Stockholm S-100 44, Sweden; ⊚ orcid.org/ 0000-0002-2346-7063; Phone: +46 73 942 66 34; Email: trosen@kth.se

Benjamin S. Hsiao – Department of Chemistry, Stony Brook University, Stony Brook, New York 11794-3400, United States; © orcid.org/0000-0002-3180-1826; Phone: +1 631 632 7793; Email: benjamin.hsiao@stonybrook.edu

#### **Authors**

Ruifu Wang — Department of Chemistry, Stony Brook University, Stony Brook, New York 11794-3400, United States

Hongrui He — Department of Chemistry, Stony Brook University, Stony Brook, New York 11794-3400, United States Priyanka R. Sharma — Department of Chemistry, Stony Brook University, Stony Brook, New York 11794-3400, United States

Jiajun Tian – Department of Chemistry, Stony Brook University, Stony Brook, New York 11794-3400, United States

L. Daniel Söderberg — Fiber and Polymer Technology
Department and Wallenberg Wood Science Center, KTH
Royal Institute of Technology, Stockholm S-100 44, Sweden;
orcid.org/0000-0003-3737-0091

Complete contact information is available at: https://pubs.acs.org/10.1021/acs.macromol.2c01035

#### Notes

The authors declare no competing financial interest.

#### ACKNOWLEDGMENTS

The authors acknowledge financial support from the National Science Foundation (NSF- DMR-2216585), Wallenberg Wood Science Center (WWSC), the Alf de Ruvo Memorial Foundation, and the Hans Werthen Foundation.

#### REFERENCES

- (1) Moon, R. J.; Martini, A.; Nairn, J.; Simonsen, J.; Youngblood, J. Cellulose nanomaterials review: structure, properties and nanocomposites. *Chem. Soc. Rev.* **2011**, *40*, 3941–3994.
- (2) Saito, T.; Nishiyama, Y.; Putaux, J. L.; Vignon, M.; Isogai, A. Homogeneous suspensions of individualized microfibrils from TEMPO-catalyzed oxidation of native cellulose. *Biomacromolecules* **2006**, *7*, 1687–1691.
- (3) Saito, T.; Kimura, S.; Nishiyama, Y.; Isogai, A. Cellulose nanofibers prepared by TEMPO-mediated oxidation of native cellulose. *Biomacromolecules* **2007**, *8*, 2485–2491.
- (4) Sharma, P. R.; Joshi, R.; Sharma, S. K.; Hsiao, B. S. A simple approach to prepare carboxycellulose nanofibers from untreated biomass. *Biomacromolecules* **2017**, *18*, 2333–2342.
- (5) Isogai, A.; Saito, T.; Fukuzumi, H. TEMPO-oxidized cellulose nanofibers. *Nanoscale* **2011**, *3*, 71–85.
- (6) Geng, L. H.; Peng, X. F.; Zhan, C. B.; Naderi, A.; Sharma, P. R.; Mao, Y. M.; Hsiao, B. S. Structure characterization of cellulose nanofiber hydrogel as functions of concentration and ionic strength. *Cellulose* **2017**, *24*, 5417–5429.
- (7) Zimmermann, T.; Bordeanu, N.; Strub, E. Properties of nanofibrillated cellulose from different raw materials and its reinforcement potential. *Carbohydr. Polym.* **2010**, *79*, 1086–1093.
- (8) Sharma, S. K.; Sharma, P. R.; Lin, S.; Chen, H.; Johnson, K.; Wang, R.; Borges, W.; Zhan, C.; Hsiao, B. S. Reinforcement of natural rubber latex using jute carboxycellulose nanofibers extracted using nitro-oxidation method. *Nanomaterials* **2020**, *10*, 706.
- (9) Sharma, P. R.; Chattopadhyay, A.; Zhan, C.; Sharma, S. K.; Geng, L.; Hsiao, B. S. Lead removal from water using carboxycellulose nanofibers prepared by nitro-oxidation method. *Cellulose* **2018**, 25, 1961–1973.
- (10) Geng, L. H.; Mittal, N.; Zhan, C. B.; Ansari, F.; Sharma, P. R.; Peng, X. F.; Hsiao, B. S.; Söderberg, L. D. Understanding the Mechanistic Behavior of Highly Charged Cellulose Nanofibers in Aqueous Systems. *Macromolecules* **2018**, *51*, 1498–1506.
- (11) Wang, R.; Rosen, T.; Zhan, C.; Chodankar, S.; Chen, J.; Sharma, P. R.; Sharma, S. K.; Liu, T.; Hsiao, B. S. Morphology and Flow Behavior of Cellulose Nanofibers Dispersed in Glycols. *Macromolecules* **2019**, *52*, 5499–5509.
- (12) Kerekes, R. J.; Schell, C. J. Characterization of Fiber Flocculation Regimes by a Crowding Factor. *J. Pulp Pap. Sci.* **1992**, *18*, 32–38.

- (13) Rosén, T.; Hsiao, B. S.; Söderberg, L. D. Elucidating the Opportunities and Challenges for Nanocellulose Spinning. *Adv. Mater.* **2021**, *33*, 2001238.
- (14) Dong, H.; Snyder, J. F.; Williams, K. S.; Andzelm, J. W. Cation-induced hydrogels of cellulose nanofibrils with tunable moduli. *Biomacromolecules* **2013**, *14*, 3338–3345.
- (15) Hirrien, M.; Desbrières, J.; Rinaudo, M. Physical properties of methylcelluloses in relation with the conditions for cellulose modification. *Carbohydr. Polym.* **1996**, *31*, 243–252.
- (16) Arvidson, S.; Lott, J.; McAllister, J.; Zhang, J.; Bates, F.; Lodge, T.; Sammler, R.; Li, Y.; Brackhagen, M. Interplay of phase separation and thermoreversible gelation in aqueous methylcellulose solutions. *Macromolecules* **2013**, *46*, 300–309.
- (17) Zhang, M.; Yang, B.; Liu, W.; Li, S. Influence of hydroxypropyl methylcellulose, methylcellulose, gelatin, poloxamer 407 and poloxamer 188 on the formation and stability of soybean oil-in-water emulsions. *Asian J. Pharm. Sci.* **2017**, *12*, 521–531.
- (18) Yeo, Y. H.; Chathuranga, K.; Lee, J. S.; Koo, J.; Park, W. H. Multifunctional and thermoresponsive methylcellulose composite hydrogels with photothermal effect. *Carbohydr. Polym.* **2022**, 277, 118834.
- (19) Xuli, F.; Chung, D. Effect of methylcellulose admixture on the mechanical properties of cement. *Cem. Concr. Res.* **1996**, 26, 535–538.
- (20) Shi, C.; Zou, X.; Wang, P. Influences of ethylene-vinyl acetate and methylcellulose on the properties of calcium sulfoaluminate cement. *Constr. Build. Mater.* **2018**, *193*, 474–480.
- (21) Tanaka, F.; Stockmayer, W. H. Thermoreversible gelation with junctions of variable multiplicity. *Macromolecules* **1994**, 27, 3943–3954
- (22) Cai, J.; Zhang, L. Unique gelation behavior of cellulose in NaOH/Urea aqueous solution. *Biomacromolecules* **2006**, *7*, 183–189.
- (23) Weng, L.; Zhang, L.; Ruan, D.; Shi, L.; Xu, J. Thermal gelation of cellulose in a NaOH/thiourea aqueous solution. *Langmuir* **2004**, 20, 2086–2093.
- (24) Roy, C.; Budtova, T.; Navard, P. Rheological Properties and Gelation of Aqueous Cellulose–NaOH Solutions. *Biomacromolecules* **2003**, *4*, 259–264.
- (25) Hansen, C. M.; Smith, A. L. Using Hansen solubility parameters to correlate solubility of C60 fullerene in organic solvents and in polymers. *Carbon* **2004**, *42*, 1591–1597.
- (26) Rosén, T.; Wang, R.; Zhan, C.; He, H.; Chodankar, S.; Hsiao, B. S. Cellulose nanofibrils and nanocrystals in confined flow: Single-particle dynamics to collective alignment revealed through scanning small-angle x-ray scattering and numerical simulations. *Phys. Rev. E* **2020**, *101*, 032610.
- (27) Rosén, T.; He, H.; Wang, R.; Zhan, C.; Chodankar, S.; Fall, A.; Aulin, C.; Larsson, P. T.; Lindström, T.; Hsiao, B. S. Cross-sections of nanocellulose from wood analyzed by quantized polydispersity of elementary microfibrils. *ACS Nano* **2020**, *14*, 16743–16754.
- (28) Rosén, T.; Mittal, N.; Roth, S. V.; Zhang, P.; Lundell, F.; Söderberg, L. D. Flow fields control nanostructural organization in semiflexible networks. *Soft Matter* **2020**, *16*, 5439–5449.
- (29) Winter, H. H.; Chambon, F. Analysis of linear viscoelasticity of a crosslinking polymer at the gel point. *J. Rheol.* **1986**, *30*, 367–382.
- (30) Desbrières, J.; Hirrien, M.; Ross-Murphy, S. Thermogelation of methylcellulose: rheological considerations. *Polymer* **2000**, *41*, 2451–2461.
- (31) Perazzo, A.; Nunes, J. K.; Guido, S.; Stone, H. A. Flow-induced gelation of microfiber suspensions. *Proc. Natl. Acad. Sci. U.S.A.* **2017**, 114, E8557–E8564.
- (32) Chevillard, C.; Axelos, M. Phase separation of aqueous solution of methylcellulose. *Colloid Polym. Sci.* **1997**, *275*, 537–545.
- (33) Rosén, T.; Wang, R.; He, H.; Zhan, C.; Chodankar, S.; Hsiao, B. S. Shear-free mixing to achieve accurate temporospatial nanoscale kinetics through scanning-SAXS: ion-induced phase transition of dispersed cellulose nanocrystals. *Lab Chip* **2021**, *21*, 1084–1095.
- (34) Rosén, T.; Wang, R.; He, H.; Zhan, C.; Chodankar, S.; Hsiao, B. S. Understanding ion-induced assembly of cellulose nanofibrillar

- gels through shear-free mixing and in situ scanning-SAXS. *Nanoscale Adv.* **2021**, *3*, 4940–4951.
- (35) Somani, R. H.; Hsiao, B. S.; Nogales, A.; Fruitwala, H.; Srinivas, S.; Tsou, A. H. Structure development during shear flow induced crystallization of i-PP: in situ wide-angle X-ray diffraction study. *Macromolecules* **2001**, *34*, 5902–5909.
- (36) Li, M. C.; Wu, Q. L.; Song, K. L.; Lee, S.; Qing, Y.; Wu, Y. Q. Cellulose Nanoparticles: Structure-Morphology-Rheology Relationships. *ACS Sustainable Chem. Eng.* **2015**, *3*, 821–832.
- (37) Surface Tension, Hansen Solubility Parameters, Molar Volume, Enthalpy of Evaporation, and Molecular Weight of Selected Liquids. https://www.accudynetest.com/solubility\_table.html (accessed 04/03/2022).
- (38) Bruel, C.; Tavares, J. R.; Carreau, P. J.; Heuzey, M.-C. The structural amphiphilicity of cellulose nanocrystals characterized from their cohesion parameters. *Carbohydr. Polym.* **2019**, 205, 184–191.
- (39) Okita, Y.; Fujisawa, S.; Saito, T.; Isogai, A. TEMPO-Oxidized Cellulose Nanofibrils Dispersed in Organic Solvents. *Biomacromolecules* **2011**, *12*, 518–522.

### **□** Recommended by ACS

#### Isotropic Gels of Cellulose Nanocrystals Grafted with Dialkyl Groups: Influence of Surface Group Topology from Nonlinear Oscillatory Shear

Sylwia Wojno, Roland Kádár, et al.

APRIL 25, 2023 LANGMUIR

READ 🗹

## Cellulose Nanocrystal Gels with Tunable Mechanical Properties from Hybrid Thermal Strategies

Zongzhe Li, Mark J. MacLachlan, et al.

JANUARY 31, 2023

ACS APPLIED MATERIALS & INTERFACES

READ 🗹

#### Crystalline and Hairy Nanocelluloses for 3D Printed Hydrogels and Strongly Structured Cryogels

Seyed Mohammad Amin Ojagh, Theo G.M. van de Ven, et al.

MARCH 28, 2023

ACS SUSTAINABLE CHEMISTRY & ENGINEERING

READ 🗹

## Nanoengineering the Redispersibility of Cellulose Nanocrystals

Breanna Huntington, Amir Sheikhi, et al.

DECEMBER 05, 2022

BIOMACROMOLECULES

READ 🗹

Get More Suggestions >